Pulsed Laser Deposition Thin Films of $Pr_{0.7}Sr_{0.3}MnO_3$: The Role of Growth Temperature

B. Mercey, J. Wolfman, W. Prellier,* M. Hervieu, Ch. Simon, and B. Raveau

Laboratoire CRISMAT, CNRS UMR 6508, ISMRA et Université de Caen, 6 Boulevard du Maréchal Juin, 14050 Caen Cedex, France

Received March 7, 2000. Revised Manuscript Received June 26, 2000

$Pr_{0.7}Sr_{0.3}MnO_3$ thin films were deposited at different temperatures on [100]-$LaAlO_3$ substrates by the pulsed laser deposition (PLD) technique. X-ray diffraction, electron diffraction, and high-resolution electron microscopy (HREM) show that the deposition temperature influences dramatically the orientation of the films and their microstructure, within a very short range. The films grown at low temperature are [101]-oriented and exhibit a columnar growth with well-connected grains. One observes the coexistence of [010]- and [101]-oriented domains poorly connected platelet-like crystals, for films deposited at high temperature. The HREM observation of a cross section of the low-temperature thin film reveals the presence of an interfacial strained layer close to the substrate, allowing a growth mechanism to be proposed. The magnetic measurements show that the Curie temperature is independent of the growth temperature. In contrast, the magnetotransport properties are strongly influenced, due to the different nature of the microstructure and especially to the role of the grain boundaries that may exhibit a depressed T_c.

I. Introduction

Colossal magnetoresistance (CMR) properties have been observed on thin film doped perovskite $La_{1-x}A_x$-MnO_3 (A = Ba, Sr, or Ca).[1−4] To utilize these materials for device applications, in the field of magnetic recording, it is necessary to obtain high-quality thin films. Among all the thin film deposition techniques, the pulsed laser deposition (PLD) technique, first developed by Diijkamp[5] for superconducting cuprates, appears the most suitable for the deposition of complex thin film oxides and thus seems well adapted for manganites. It allows indeed one not only to have the cationic composition but also to better control the oxygenation of these materials than the other techniques.[6] For these reasons attractive results have been obtained to date for thin films of superconducting cuprates and manganites.[7] It is well-known that the magnetic and transport properties of maganite thin films are strongly dependent on the growth and annealing conditions. As a consequence, significant efforts have been carried out to optimize a postannealing procedure to obtain high magnetoresistance (MR) values.[8−9]

In this article, we report the synthesis and characterization of as-grown $Pr_{0.7}Sr_{0.3}MnO_3$ thin films, i.e., with no annealing, using the PLD technique. We have precisely studied the influence of the deposition temperature upon the structural characteristics of the films. We show that the temperature influences not only the growth direction of the film but also the microstructure of the material, which differ in particular by the nature and the amount of the grain boundaries present. At the end, we correlate the magnetotransport properties of these films with their microstructures.

II. Experimental Section

Targets with composition $Pr_{0.7}Sr_{0.3}MnO_3$ were prepared by a solid-state reaction. A stoichiometric mixture of well-ground Pr_6O_{11}, $SrCO_3$, and Mn_2O_3 powders was calcinated at 900 °C for 10 h. After grinding, the resultant powder was fired at 950 °C for 15 h in air. The powder was ground again and then pressed into a pellet and sintered at 1500 °C for 16 h.

A pulsed KrF excimer laser (Lambda Physik LPX200, λ = 248 nm) was utilized for the film deposition. The substrate was [100] $LaAlO_3$ whose crystallographic structure is pseudocubic (actual rhombohedral structure **a** = 3.788 Å and α = 90°4[10]). The substrate directions are indexed "S" (subscript), considering the cubic perovskite subcell. The details of the geometry of the experiment have been previously described.[11] Briefly, a rotating target is positioned in front of the laser beam to produce a plume of ablated material perpendicular to the

(1) Von Helmolt, R.; Wecker, J.; Holzapfel, R.; Schultz, L.; Samwer, K. *Phys. Rev. Lett.* **1993**, *71*, 2331.
(2) Kuster, R. M.; Singleton, J.; Keon, D. A.; Greedy, R. M.; Hayes N. *Physica B* **1989**, *155*, 362.
(3) McCormack, M.; Jin, S.; Tiefel, T. H.; Fleming, R. M.; Phillips, J. M.; Ramesh, R. *Appl. Phys. Lett.* **1994**, *64*, 3045.
(4) Ju, H. L.; Kwon, C.; Li, Q.; Greene, R. L.; Venkatesan, T. *Appl. Phys. Lett.* **1994**, *65*, 2108.
(5) Diijkamp, D.; Venkatesan, T.; Wu, X. D.; Shaheen, S. A.; Jinawi, N.; Minke-Lee, Y. H.; Croft, M. *Appl. Phys. Lett.* **1987**, *51*, 619.
(6) Chrisey, D. K.; Hubler, G. K. *Pulsed Laser Deposition of Thin Films*; Wiley-Interscience: New York, 1994.
(7) See for example: Venkatesan, T.; Rajeswari, M.; Dong, Z.-W.; Ogale, S. B.; Ramesh, R. *Philos. Trans. R. Soc. London* **1998**, *356*, 1661. Prellier, W.; Biswas, A.; Rajeswari, M.; Venkatesan, T.; Greene R. L. *Appl. Phys. Lett.* **1999**, *75*, 397. Norton, D. P.; Chakoumakos, N. C.; Budai, J. D.; Lowdes, D. H.; Sales, B. C.; Thompson, J. R.; Christen, D. K. *Science* **1994**, *265*, 2074.
(8) Wagner, P. W.; Metlushko, V.; Trappeniers, L.; Vantomme, A.; Vanacken, J.; Kido, G.; Mohshalkov, V. V.; Bruynseraede, Y. *Phys. Rev. B* **1997**, *55*, 3699.
(9) Gangapadhyay, S.; Cross, R. W.; Elliner, G.; Jackson, S.; Jenner, A. G.; Greenough, R. D.; Dyer, P. E.; Bao, X.; Metzer, R. M.; Parker, M. R. *Magn. Mater. Lett.* **1995**, *145*, 225.
(10) Roth, R. S. *J. Res. NBS, RP* **1957**, *58*, 2736.
(11) Allen, J. L.; Hervieu, M.; Mercey, B.; Hamet, J. F.; Raveau, B. *J. Mater. Chem.* **1996**, *6*, 1141.

10.1021/cm000206z CCC: $19.00
Published on Web 09/21/2000

substrate. The distance between the target and the substrate is around 5 cm. The beam, directed into the deposition chamber with an angle of 45°, is focused onto the target with an energy density of 2 J/cm^2. The repetition rate is 4 Hz. The heater was kept at a constant temperature ranging from 600 to 700 °C during deposition. Depositions are carried under 0.4 mbar of flowing oxygen. After deposition, the samples are slowly cooled to room temperature under an oxygen pressure of 500 mbar. The deposition rate is around 0.9 Å/pulse and the typical thickness is 6500 Å. Optimized films (i.e., with the highest Curie temperature) are obtained without further ex situ annealing at high temperature. The film is deposited just after the expected temperature has been reached to avoid surface contamination.

The structural study was carried out by X-ray diffraction using a Seifert XRD 3000P diffractometer with Cu Kα_1 radiation ($\lambda = 1.5405$ Å) for the $\theta-2\theta$ measurements. The step used is 0.02° with a counting time of 1 s. The film levelness is checked by adjusting the position of the two most intense diffraction peaks of the substrate by a rocking curve. The error in the interreticular distances is around 0.01 Å. The electron diffraction (ED) observation was made with a JEOL 200 CX microscope; the reciprocal space was reconstructed by tilting around the crystallographic axes, especially the equivalent $[010]_p$* and $[101]_p$* directions of the perovskite subcell. The high-resolution electron microscopy (HREM) was carried out with a TOPCON 002B microscope, having a point resolution of 1.8 Å. The two microscopes are equipped with an energy dispersive scattering (EDS) analyzer to check the composition of the films. Magnetization and transport measurements were performed with a Quantum Design SQUID magnetometer (MPMS) and physical properties measurement system (PPMS), respectively.

III. Results

Various growth conditions were tested during this study. To illustrate the influence of the deposition process on the nature of the as-deposited thin films, two types of samples are detailed herein. They have been prepared using two processes, which only differ by the deposition temperature, namely, 620 and 640 °C. They are, hereafter, referred to as the low-temperature (LT) and high-temperature (HT) forms, respectively. We chose these two sets of films because they were very representative of what we found. Films below 620 °C look the same at the film we have studied (LT phase). Films above 640 °C are identical to the one deposited at 640 °C (HT phase). Moreover, because they are at the boundary, we think that it is interesting to look at them in more detail (from a structural and physical point of view). This will also illustrate how the synthesis of the manganites is very sensitive to the growth conditions and that a small difference can lead to drastic changes in the properties.

(1) Structural Properties. (1.1) Low-Temperature Phase (LT). (a) X-ray Diffraction Study. A typical XRD pattern of the LT films is shown in Figure 1. Besides two diffraction peaks from the substrate, four peaks are observed. They can be indexed considering the coexistence of two different systems. The most intense peaks, labeled LT1 and LT2, whose sharpness indicates the high crystallinity of the films, are observed at $2\theta = 23.02°$ and 47.02°, respectively. They are assumed to belong to the majority phase and could be attributed to the 100 and 200 reflections of a perovskite subcell having an $a_P = 3.86$ Å lattice parameter. The less intense peaks, labeled LT3 and LT4, are observed at $2\theta = 22.78°$ and 46.30°, respectively. They could also be attributed to the 100 and 200 reflections of a second perovskite system, having $a_P = 3.91$ Å as the lattice parameter.

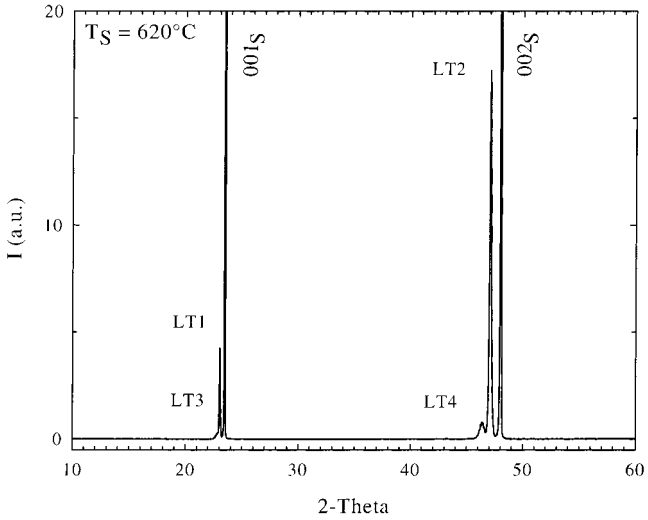

Figure 1. X-ray diffraction pattern of the LT phase. Intensity is given in arbitrary units. Index S denotes peaks of the $LaAlO_3$ substrates.

Referring to the orthorhombic *Pnma*-type lattice parameters of the bulk material,[12] $a = 5.486(3)$ Å ($a_P\sqrt{2}$), $b = 7.713(5)$ Å ($2a_P$), $c = 5.467(3)$ Å ($a_P\sqrt{2}$), the d_{020} and d_{101} distances are 3.856 and 3.872 Å, respectively. The a_P subcell parameter of the first perovskite system, determined from the intense LT1 and LT2 peaks, fits rather well with the above values. However, LT1 and LT2 values do not provide precise information on the orientation of the films. Moreover, the LT3 and LT4 peaks (3.91 Å) cannot be simply indexed with these parameter values.

Assuming that the thin films also adopt the $GdFeO_3$ -type structure, two orientations of the film, with respect to the substrate, could fit the $a_P = 3.86$ Å determined from the XRD diffraction data (LT1 and LT2 peaks):

(i) If the film is [010]-oriented, peaks labeled LT1 and LT2 correspond respectively to 020 and 040 reflections ($0k0$: $k = 2n$).

(ii) If the film is [101]-oriented, LT1 and LT2 peaks correspond respectively to 101 and 202 reflections.

One must keep in mind that differences between lattice parameters are often observed when the same phase is prepared in bulk form or in thin film form.[14] Two main features can generate such lattice parameter variations. First, there may exist strains induced by the difference between substrate and film lattice parameters. Second, the oxygen content may vary, which also would induce lattice parameter variations. Taking into account a possible slight variation of the lattice parameters, the orientation of the film with respect to the substrate cannot be unambiguously determined from the XRD data because the observed values for LT1 and LT2 peaks can fit both film orientations. Furthermore, as mentioned before, the second perovskite system (LT3 and LT4 peaks) does not correspond to the expected

(12) Knizek, K.; Jirak, Z.; Pollert, E.; Zounouva, F.; Vratislav, S. *J. Solid State Chem.* **1992**, *100*, 292.
(13) Krishnan, K. M.; Modak, A. R.; Lucas, C. A.; Michel, R.; Cherry, H. B. *J. Appl. Phys.* **1996**, *79*, 5169.
(14) Mercey, B.; Lecoeur, Ph.; Hervieu, M.; Wolfman, J.; Simon, Ch.; Murray, H.; Raveau, B. *Chem. Mater.* **1997**, *9*, 1177.

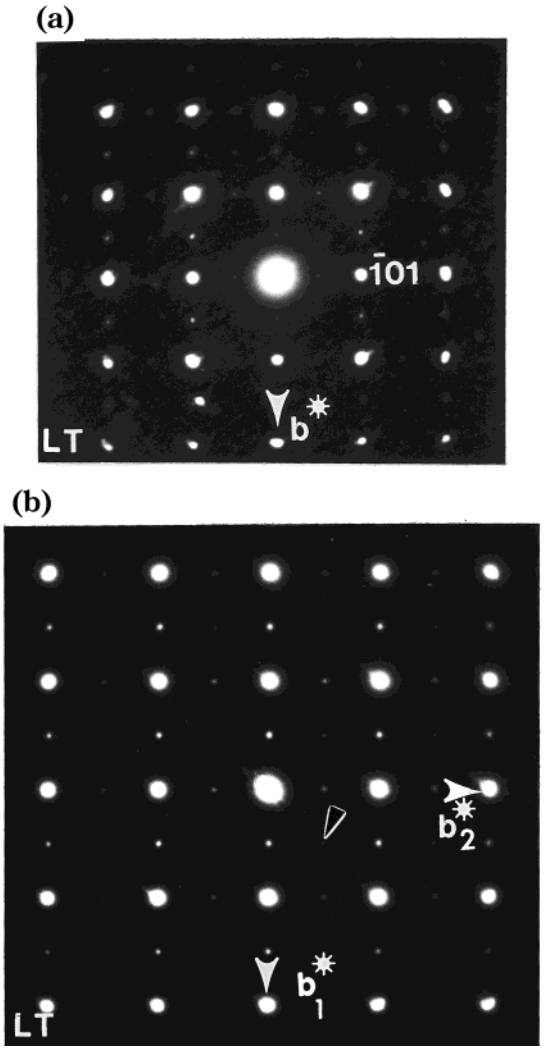

Figure 2. ED pattern of the LT phase recorded along the direction perpendicular to the substrate plane: (a) this pattern shows what is typical of a [101] zone axis of a *Pnma*-type structure; (b) this pattern shows the 90°-oriented domains (index as 1 and 2).

interreticular distances. A transmission electron microscopy study is necessary to determine the orientation of the film.

(b) Electron Diffraction Study. The EDS analyses carried out on numerous areas of the films confirmed the homogeneity of the film composition, close to that of the target, i.e., the nominal one $Pr_{0.7}Sr_{0.3}Mn$.

The reconstruction of the reciprocal space carried out, by tilting around [010]* and [101]*, confirms the lattice parameters $a = a_P\sqrt{2}$, $b = 2a_P$, and $c = a_P\sqrt{2}$. The system of intense reflections determined from the largest domains is in agreement with that observed for the bulk material ($0kl$: $k + l = 2$ and $hk0$: $h = 2n$). However, the ED patterns are often more complex, due to the existence of 90°-oriented domains (see further).

Figure 2a shows a typical electron diffraction (ED) pattern, recorded along the direction perpendicular to the substrate plane, $[001]_S$. It is characteristic of the [101] zone axis of the *Pnma*-type structures. Note that this ED pattern shows that the structure and orientation of the LT film are similar to the ones observed for $Pr_{0.7}Ca_{0.3-x}Sr_xMnO_3$ ($x = 0.05$ and $x = 0.08$) grown by sputtering deposition.[14]

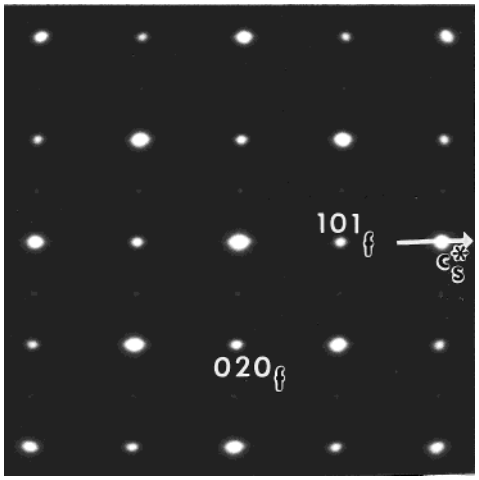

Figure 3. ED of the cross section of the LT phase.

The ED study allows for two results to be obtained. First, it reveals the [101] orientation of the film with respect to the substrate, and second it reveals that the [101]-oriented film is composed of 90°-oriented domains. As an example, two variants are superimposed in Figure 2b. The b_1 and b_2 axes of these domains are aligned along either the $[100]_S$ or the $[010]_S$ directions of the substrate. Moreover, in a few parts of the film, the ED patterns, recorded along the $[001]_S$ direction, exhibit very weak additional reflections (marked with small arrows in Figure 2b). These very weak, scarcely visible, extra spots can be generated by a double diffraction effect or, likely as mentioned in ref 14, by the presence of more or less extended [010]-oriented regions. Both types of oriented domains have a common origin. They directly result from the distortion of the perovskite subcell and are commonly observed in the *Pnma*-type manganites.[10] In a general way, these microstructural features are strongly dependent on the lattice parameter relationships $a/\sqrt{2} \sim b/2 \sim c/\sqrt{2} \sim a_P$. The influence of the substrate strain effects will be further discussed.

The ED patterns of the cross-section samples show that the film and the substrate are perfectly aligned. They also clearly evidence the small discrepancy between the film and substrate lattice parameters. The periodicity measured along the direction perpendicular to the substrate is close to 3.86 Å (Figure 3), in agreement with the X-ray diffraction data. Within the substrate plane, one observes spots, which imply a doubling of the a_P parameter along one direction (Figure 3); this in agreement with the existence of domains having their *b*-axis parallel to the substrate plane. The lattice parameter of the film, measured on the ED patterns taking 3.86 Å as standard for the perpendicular vector, is 3.8 Å. In the same way, the absence of such a doubling of the a_P parameter along a direction perpendicular to the substrate plane is in agreement with the [101] orientation of the film. It also attests to the absence (or at least the rareness) of [010]-oriented areas.

From these observations, one can conclude that the low-temperature form of the $Pr_{0.7}Sr_{0.3}MnO_3$ film retains a $GdFeO_3$-type distortion of the perovskite. The film is [101]-oriented and the [010] and $[10\bar{1}]$ film directions are aligned with the $[100]_S$ and $[010]_S$ directions of the substrate, respectively. The [010], [101], and $[10\bar{1}]$ are perpendicular to one another, with $d_{101} \approx 3.86$ Å and

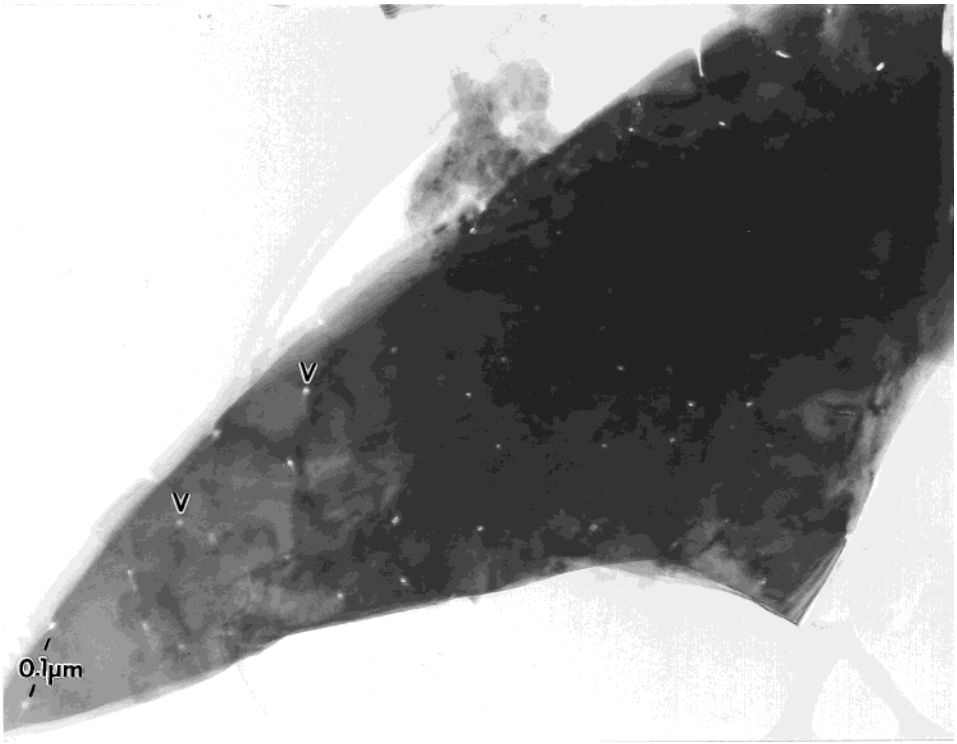

Figure 4. Overall HREM image recorded along the $[001]_S$ of a crystal belonging to the LT phase (V denotes small voids between the grain boundaries).

$d_{020} \approx d_{10\bar{1}} \approx 3.81$ Å. These orientation relationships, and especially the difference between d_{101} and $d_{10\bar{1}}$, imply that the actual cell of the $Pr_{0.7}Sr_{0.3}MnO_3$ film is not orthorhombic but monoclinic. The calculated β angle is close to 90.6°. This distortion is induced by the substrate strain, resulting from the parameter mismatch between film and substrate. A similar effect has been reported for other thin films with a $GdFeO_3$-type structure, particulary, $Pr_{0.5}Ca_{0.5}MnO_3$[15] and $La_{0.7}Sr_{0.3}MnO_3$.[16]

In the course of the ED characterization of the LT films, no secondary phase or precipitates, which could be associated with the LT3−LT4 peaks ($a_P = 3.91$ Å), have been detected.

Besides the origin of this second system, these results raise two issues. The first one deals with the in-plane parameters of the substrate and those of the film. It indeed appears that the average a_P in-plane parameters of the film are in fact a "mid term" value between the $a_S = 3.788$ Å parameter of the substrate and the $\bar{a}_P \approx 3.87$ Å parameter of the bulk phase. Note that previous observations do not often report the occurrence of a "mid-term" value of the film parameters. Usually, for manganite thin films grown by pulsed laser deposition, the in-plane lattice parameters of the first layers of the film fit exactly the lattice parameters of the substrate. Therefore, investigations of the interface become essential. The second issue deals with the cell volume. Referring to the bulk material,[12] the cell volume is 231.3 Å^3, i.e., 57.8 Å^3, per perovskite unit. Although the ED patterns do not provide high accuracy, the film cell volume deduced from the above-measured and -calculated parameters, 56.1 Å^3, is significantly smaller. Such a deviation could be correlated to an effect of the manganese oxidation state. Knizek et al.[12] indeed evidenced a cell volume decreasing from 57.2 Å^3 for $Pr_{0.6}Sr_{0.4}MnO_{2.984}$ to 56.7 Å^3 for $Pr_{0.6}Sr_{0.4}MnO_{3.019}$. These issues will be discussed in more detail hereafter.

(c) Microstructural and Nanostructural Study along $[001]_S$. The HREM images, viewed along $[001]_S$, confirm the good crystallinity of the films, expected from the quality of both XRD and ED data. As seen in the overall images (Figure 4), films are formed of small grains about 0.1-μm large. An enlarged image is given in Figure 5, where the positions of the heavy cations are imaged as bright dots. These images show that each grain exhibits the 90°-oriented domains detected by ED. Two types of boundaries are thus observed in the LT films, twinning boundaries within the grain and normal grain boundaries (GB).

(i) Domains Boundaries (DB). The microstructure of the film clearly exhibits a difference with regard to that of the bulk material.[12] In the bulk, one indeed observed all the variants generated by the setting up of the distortion along the equivalent directions of the perovskite subcell. In the films, all the characterized domains correspond to the alignment of the b axes ($b = 2a_P$) alternately along $[100]_S$ and $[010]_S$. Only very few and very small [010]-oriented zones have been observed close to the grain boundaries. This point is closely related to the geometrical relationships between the parameters and emphasizes a particular role of the substrate through the distortion of the perovskite cell. In the film, $d_{101}/d_{020} \sim 1.013$ whereas $d_{020}/d_{10\bar{1}} \sim 1.00$. The first ratio, significantly different from 1 for a perovskite distortion, explains why the [010] domains are not favored. In contrast, because $d_{020} \sim d_{10\bar{1}}$, the superstructure takes place along $[100]_S$, as well as

(15) Haghiri-Gosnet, A. M.; Hervieu, M.; Simon, Ch.; Mercey, B.; Raveau, B., unpublished material.
(16) Haghiri-Gosnet, A. M.; Wolfman, J.; Mercey, B.; Simon, Ch.; Lecoeur, Ph.; Korzenski, M.; Raveau, B., unpublished material.

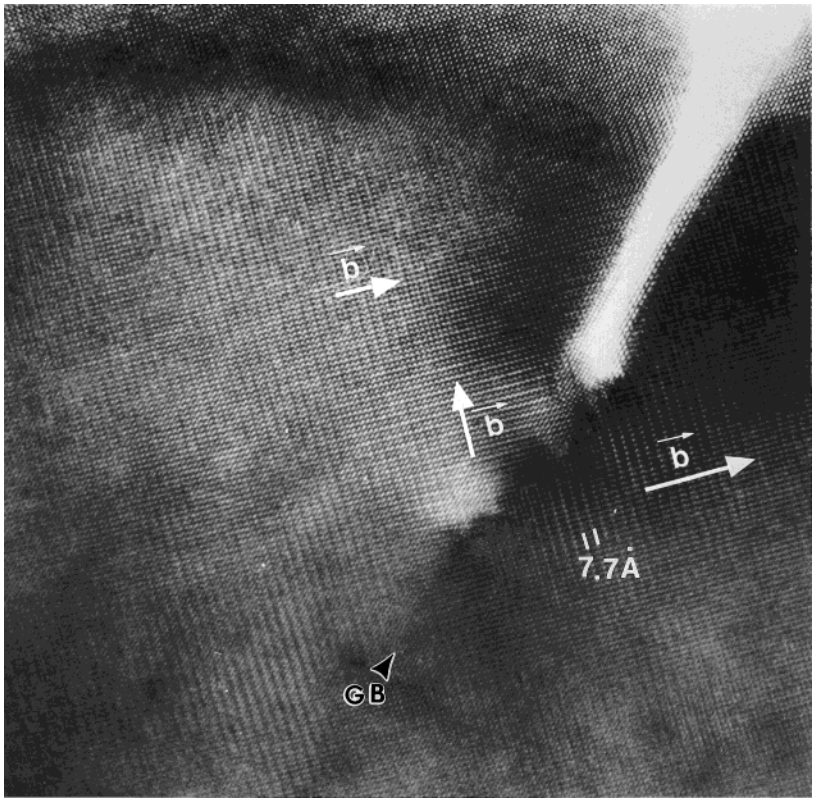

Figure 5. Enlarged image of the LT phase. Note the relationships between 2 in-plane parameters showing a grain boundary. The position of the heavy cations are imaged as bright dots.

$[010]_S$, with incoherent boundaries. This is clearly observed in Figure 5. Note that the role of the substrate and thermal process has already been discussed in superconducting cuprate thin films having an *a*-axis orientation.[17,18]

(ii) Grain Boundaries (GB). These remarkable relationships between the two perpendicular in-plane parameters favor a high quality of the grain boundaries (GB). The GBs are scarcely visible in the images (Figure 4), attesting to a strain-free junction. The only deviation with regard to a perfect [101] film structure is the existence of the tiny [010] zones at the neighboring regions of the grain boundaries. As discussed above, it can be assumed that the parameter mismatch is more easily accommodated in these areas. At the junction point between grain boundaries, small voids are observed (labeled V in Figures 4 and 6), but no ill-crystallized zones or secondary phases have been detected at this level.

As mentioned above, the experimental through-focus series are very similar to those observed in the bulk material[12] and thus confirm the structure type of this manganese oxide deposited in the form of thin film. Moreover, we observe, as in bulk material, the systematic presence, in the thinner part of the grains, of pointlike defects which appear, in Figure 6, as dark areas in the matrix. The existence of such phenomena has already been reported and discussed[19] and they were correlated to the formation of $A^{II}Mn^{IV}O_3$ clusters, running along a few octahedra long. Note that dislocations are sometimes produced in the neighboring of the GB (noted D in Figure 6).

Numerous grains of the films prepared under the previously described conditions were carefully characterized. They do reveal the absence of precipitate or extended defects (such as the formation of rock salt-type layers[15,20]).

(d) Microstructural Study along $[110]_S$. Viewing the film along $[100]_S$ or $[010]_S$ allows one to characterize the substrate/film interface, observe the nature of the interfacial zone, and also detect any structural features along the growth axis. The existence of interfacial slices, which is of high interest, has already been evidenced in manganese oxide thin films.[20,21]

The overall low-resolution image of a cross section (Figure 7), viewed along the $[110]_S$ direction of the substrate, exhibits average film thickness, which is in agreement with that determined from profilometer measurements (≈7000 Å). It shows that the entire thickness of the film is observed. Due to the large scale, Figure 7 presents two parts of a cross section view (separated by a dotted line), selected close to the top part of the film and the interfacial zone. Two zones are clearly visible in these images: a zone exhibiting a contrast different from that of the rest of the film is located at the interface, whereas the upper part of the film exhibits a characteristic columnar growth.

In the upper part, the film is constructed of 300−500-Å wide columns closely connected. This observation

(17) Allen, J. L.; Mercey, B.; Prellier, W.; Hamet, J. F.; Hervieu, M.; Raveau, B. *Physica C* **1995**, *241*, 158.
(18) Hamet, J. F.; Blanc-Guilhon, B.; Taffin, A.; Mercey, B.; Hervieu, M.; Raveau, B. *Physica C* **1993**, *214*, 55.
(19) Hervieu, M.; Van Tendeloo, G.; Caignert, V.; Maignan, A.; Raveau, B. *Phys. Rev. B* **1996**, *53*, 14274.
(20) Lebedev, O. I.; Van Tendeloo, G.; Amelinckx, S.; Leubold, B.; Habermeir H. U. *Phys. Rev. B* **1998**, *58*, 8065.
(21) Mercey, B.; Salvador, P. A.; Prellier, W.; Doan, T. D.; Wolfman, J.; Hamet, J. F.; Hervieu, M.; Raveau B. *J. Mater. Chem.* **1999**, *9*, 233.

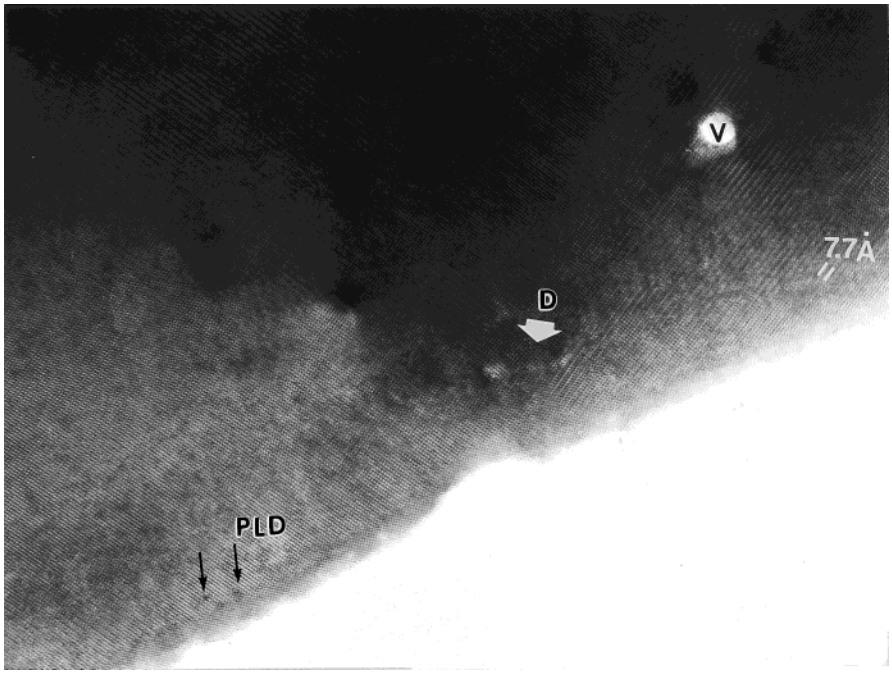

Figure 6. Enlarged image of the LT phase. V and D denote respectively small voids and a dislocation in the film.

is in agreement with the images recorded along the column axis. These images provide another interesting piece of information because they confirm the absence, or at least the very small number, of [010]-oriented domains in the whole thickness of the film. Though the exact nature of the grain boundaries can hardly be determined viewing the columns along that direction, the voids detected in Figure 3 do correspond to the separation between two or three adjacent columns, without any secondary phase.

A columnar growth of thin films is generally correlated with a relaxation process. As it is not observed close to the interface of the present LT films, this column-free zone is correlated with the presence of an interfacial strained layer. This strain is supposed to be generated by the fact that the in-plane a_P parameters of the film perfectly match those of the substrate, namely, $a_S = 3.788$ Å, as observed in the images. Assuming that the volume cell mainly depends on the composition of the sample and that this volume is constant for the whole film (56.1 $Å^3$ in the present film), the perpendicular parameter is calculated to 3.91 Å, which exactly fits with the measured value for the LT3 and LT4 peaks.

The electron microscopy results allow us to propose the following growth mechanism. At the interface, a strained interfacial layer is deposited; the strain effects are due to accommodation of the substrate and film parameters, despite their mismatch (≈3.87 vs 3.788 Å, respectively). The cell parameters of the strained structure are 3.788 × 3.788 × 3.91 Å and correspond to the second perovskite system detected by X-ray diffraction. This slice is about 450-Å thick, and beyond this point, a relaxation process is engaged so that the in-plane parameters of the film increase whereas the perpendicular parameter decreases: 3.81 × 3.81 × 3.86. This mechanism involves a columnar growth of the relaxed film.

(1.2) High-Temperature Phase (HT). (a) X-ray Diffraction Study. One typical example of the high-temperature phase is the film deposited at 640 °C, keeping the other growth conditions similar. Their XRD patterns are given in Figure 8. Positions (in 2θ units) of the principal diffraction peaks are roughly the same as those observed for the low-temperature phase. Four peaks labeled HT1, HT2, HT3, and HT4 are still observed but they are shifted toward the low 2θ values. Two peaks HT1 and HT2 are slightly shifted. This indicates a small increase of the interplanar distance along the [101] direction (3.87 vs 3.86 Å). This small change can be explained by the higher growth temperature, which can lead to a slightly different oxygenation of the film.

One important feature must be outlined. The HT3 and HT4 peaks are significantly shifted toward smaller 2θ angles, the lattice parameter of the second system being refined to $a_P = 3.96$ Å.

(b) Microstructural Study. All our attempts to prepare ion milled thinned samples failed, suggesting a strong film flimsiness. The only way to characterize the film was to take it off the substrate and to follow the conventional technique of sample preparation for electron microscopy. Even in these conditions, it was impossible to find one film fragment still attached to the substrate; this point reinforces our first hypothesis.

The low-resolution electron microscopy images show that the high-temperature films are made of poorly connected platelet-like crystals (Figure 9). The EDS analyses confirm that, in the limit of accuracy of the technique, the composition of the HT film is similar to that of the LT film.

The ED patterns, recorded along a direction perpendicular to the platelet planes (Figure 10), show sharp diffraction spots, indicating good crystallinity. They show that the crystallites are mainly [101]-oriented. However, the presence of the aforementioned additional intense spots, with regard to those observed in the LT films, suggests the existence of more extended [010]-oriented areas (small arrows in Figure 10). Our previous study on $La_{0.67}Sr_{0.33}MnO_3$ thin films showed that this

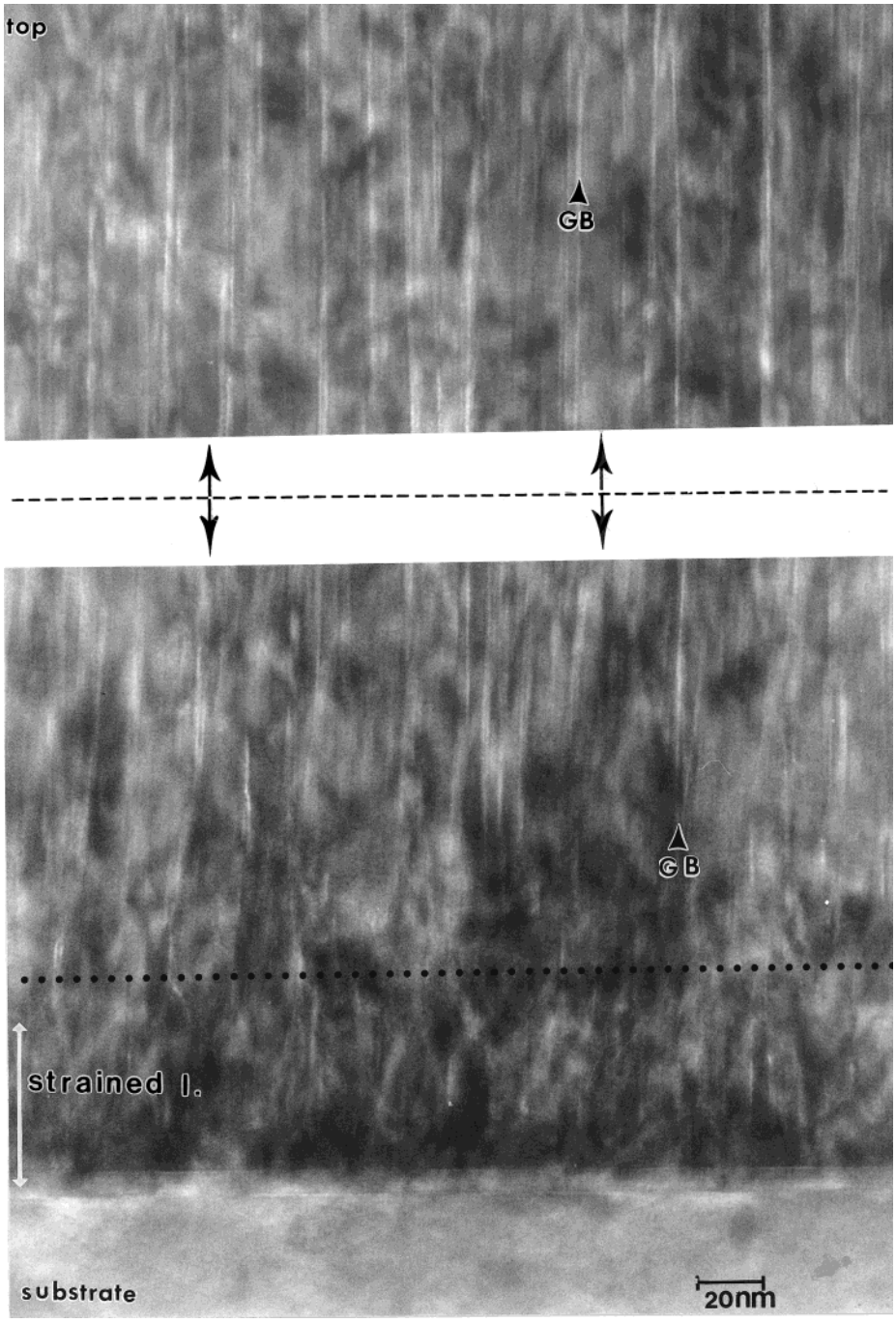

Figure 7. Two enlarged parts of the bright field image of the cross section of the LT film. The bottom part corresponds to the substrate/film interface and the top part to a zone close to the upper part of the film. GBs appear as the bright lines, except in the interfacial zone (strained layer).

feature was not observed on films deposited under standard conditions, but was generated by using a high oxygen pressure process.

The reconstruction of the reciprocal space confirms that the cell parameters are close to those observed in the LT films, $\mathbf{a} = \sqrt{2}a_P$, $\mathbf{b} = 2a_P$, and $\mathbf{c} = \sqrt{2}$, and the reflection conditions are unchanged. The contrast of the high-resolution images also confirmed that the structural type of the high-temperature phase is $GdFeO_3$-type, similar to that of the film LT form and bulk material. One example is given in Figure 11, where the contrast can be directly compared to that in Figure 5. However, this HREM study evidences several important differences between the LT and HT films:

(1) Numerous, rather large, [010]-oriented domains are formed within the [101] areas; this is clearly observed in Figure 11.

(2) The relative orientation of the [101]-oriented areas with regard to the growth axis of the crystallites is modified. In the LT form, the growth axis of the column is only [101]. In the HT form, the long axis is mainly [010], at least in a large part of the crystallites.

(3) The nature of the grain boundaries (GB) is different (Figure 9). In the HT form, wide spaces are observed between the platelets. In most of the boundaries, they are empty but sometimes a small amount of hexagonal perovskite is observed in the borderline between two adjacent platelets. The formation of this

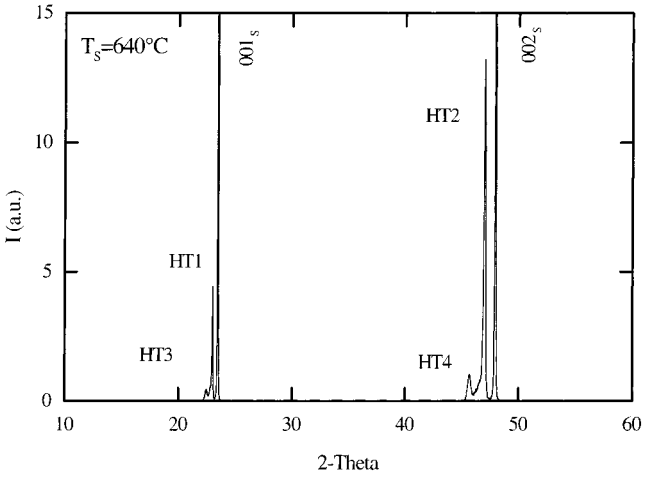

Figure 8. X-ray diffraction pattern of the HT phase. Intensity is given in arbitrary units. Index S denotes peaks of the $LaAlO_3$ substrates.

very local phase may result from a partial thermal decomposition of the manganite.

The nature of the GBs is, by itself, an explanation for the high brittleness of these HT films. The consequences are therefore double: the complete structural study could not be performed because the cross section preparation was unsuccessful and it could have a drastic influence on the transport properties.

At this point, we do not know whether the platelets are perpendicular or parallel to the substrate plane. Thus, a columnar growth seems likely impossible, in the absence of ED proof, to conclude on the actual orientation of the platelets with regard to the substrate plane. Nevertheless, the HREM study shows that, contrary to the LT film, there necessarily exists [010]- and [010]-oriented domains in the high-temperature film.

Coming back to the cell parameters, the existence of the small and numerous [010]- and [010]-oriented domains suggests that the three a_P parameters of the HT film are now very close and, moreover, close to the parameter perpendicular to the substrate, $a_P \approx 3.87$ Å (determined from XRD data). Note that this average a_P value is very close to that observed for the bulk material and it also implies a small increase of the cell volume.

The quasi-absence of an interfacial zone is also in agreement with the fact that the synthesized phase is very close to the bulk phase because no strain effects are imposed, as though the film, made of roughly connected crystallites, was only laid down on the substrate.

This means that a change in the growth temperature induces, like for the cuprates,[18] a change in the film orientation. A rather small amplitude of ΔT (≈20 °C) involves, on the one hand, this variation in the nanostructure and, on the other hand, drastic changes in the microstructure, especially at the level of the film/substrate connection and of the quality of the grain boundaries.

(2) Physical Properties. The above microstructural study of the LT and HT films shows that they both exhibit a $GdFeO_3$-type perovskite structure and a common composition. The two films differ in fact by their relative orientation, i.e., [101] LT film and mixed [101] and [010] HT film, and the quality of the grain boundaries. These characteristics are favorable for understanding the physical properties. Note that the transport properties were performed on different films and similar results were obtained each time. Thus, we report only in this section the results on two films, the same as those previously studied for their microstructures (LT and HT phases).

(2.1) Magnetic Properties. Manganese oxides with a Mn^{3+}/Mn^{4+} ratio equal to 0.7/0.3 usually undergo a transition from a low-temperature ferromagnetic-metallic state to a high-temperature paramagnetic-insulating state. It is indeed the case for the compound $Pr_{0.7}Sr_{0.3}MnO_3$, which exhibits a Curie temperature (T_C) of 285 K in bulk form.[12] The variation of the magnetization as a function of the temperature registered under a magnetic field of 0.5 T is displayed in Figure 12 for the HT and LT films. An identical Curie temperature of 265 K could be extrapolated for both films. The drop of T_C in the films compared to the that of the bulk form has often been observed in manganites and is a consequence of either slightly different oxygen content or strain-induced distortions originating from the cell parameter mismatch between the film and substrate. It should be emphasized that magnetization values are obtained assuming a homogeneous magnetization in the films. As two different growth modes associated with specific strains have been evidenced in our films, magnetic

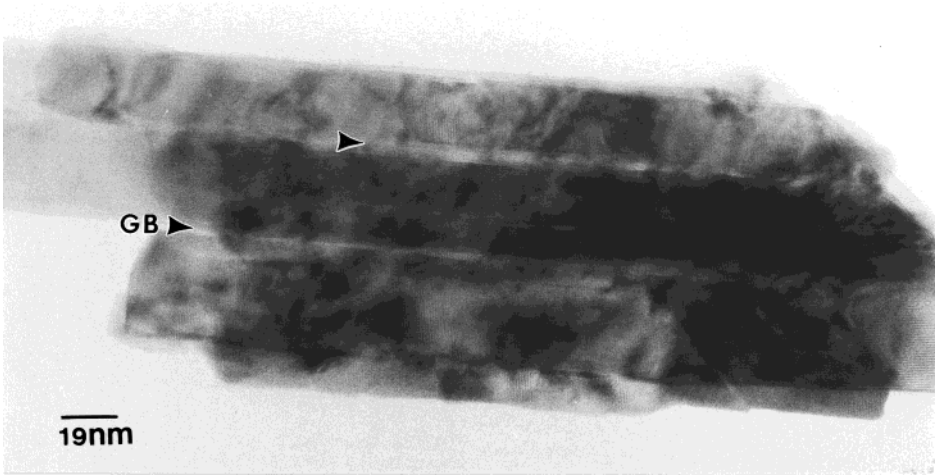

Figure 9. Low-resolution image of the HT phase showing that the film grown in a platelet-like crystals taken along the direction perpendicular to the substrate plane.

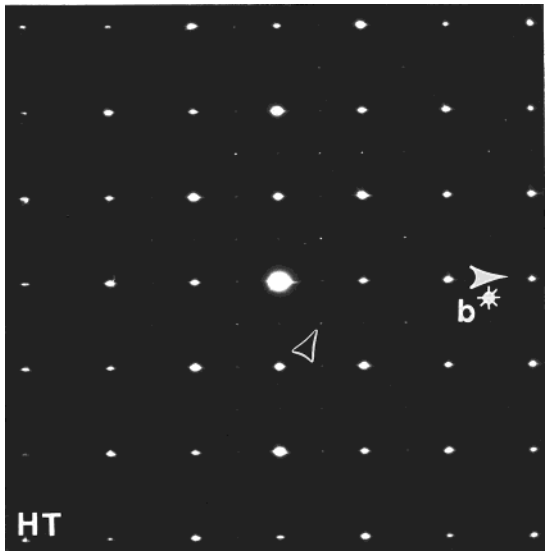

Figure 10. ED pattern taken along the direction perpendicular to the substrate plane (i.e., perpendicular to the platelet planes) of the HT phase. The small arrow corresponds to the existence of [010]-oriented domains.

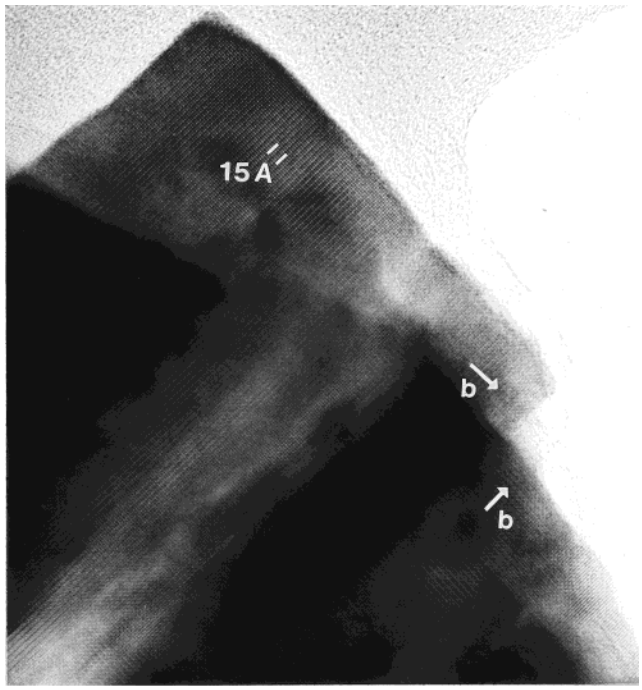

Figure 11. HREM image of the HT phase taken along a direction perpendicular to the substrate plane.

properties are likely to vary across the film. The easy axis may be different in the strained and in the relaxed part of the film. However, the thickness of the interfacial strained layer (450 Å) is small compared to the total thickness of the film (7000 Å), so that the detected magnetic signal mostly originates from the relaxed parts of the films. The similar Curie temperatures and very close perpendicular cell parameters, deduced from LT1,2 and HT1,2 peaks, indicate that the oxygen content should also be very close in the two films, despite the different growth temperatures.

(2.2) Transport Properties. Since the beginning of the study on the CMR materials, the origin of the CMR effect has been assigned to the grain boundaries.[22] In particular, Gupta et al. have shown that the grain size

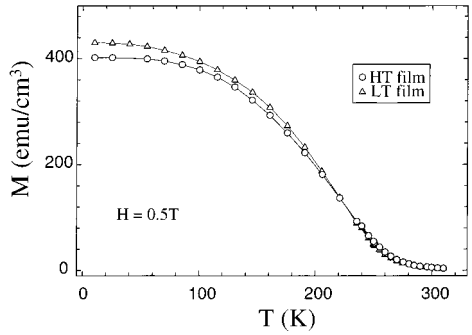

Figure 12. Magnetization versus temperature recorder under a magnetic field of 5000 Oe. The field is applied parallel to the film.

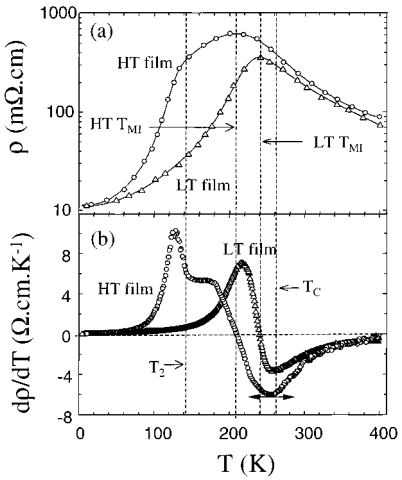

Figure 13. (a) Resistivity versus temperature for the LT phase and the HT phase. (b) Differential of the resistivity versus temperature for the LT phase and the HT phase. T_C indicates the Curie temperature for the films. See text for details.

plays an important role and that there is a huge difference, in terms of transport properties, between a polycrystalline and an epitaxial thin film.[22] They claim that the crystalline disorder induces local disorder at the grains boundaries. For these reasons and from views of the microstructure of our films, we have focused our explanation on the grains boundaries. In fact, electronic transport in these columnar films occurs through regions with possibly different mechanisms: there is conduction inside the columns and through grain boundaries (GB) between adjacent columns. The measured resistance thus depends on the intrinsic resistivity of the material and on the extrinsic resistivity associated with the GB. In the latter case, several mechanisms of conduction have been proposed, like tunneling through insulating GB, scattering by magnetically frustrated (spin glass-like) GB, or more simply double exchanging (DE) in GB with a depressed Curie temperature. The morphology of the GB strongly differs between HT and LT films, and the associated resistivities should also be quite different. The temperature dependence of the resistivities of the two films is shown in Figure 13a. For temperatures between T_C and $T = 400$ K, the measured resistivity of both HT and LT films could be fitted to

(22) Gupta, A.; Gong, G. Q.; Gang, X.; Duncombe, P. R.; Lecoeur, P.; Trouilloud, P.; Wang, Y. Y.; Dravid, V. P.; Sun, J. Z. *Phys. Rev. B* **1996**, *54*, R15629. Li, X. W.; Gupta, A.; Xiao, G.; Gong, G. Q. *Appl. Phys. Lett.* **1997**, *71*, 1124.

either an activated or a variable range hopping law, as it is usually the case in single crystals for such a small temperature range. Thus, no specific temperature dependence of the GB's resistivity could be evidenced. However, the absolute resistivities of the HT and LT films are 2 orders of magnitude higher than the resistivity of single crystals.[23] It is worth noticing that the resistivities of LT and HT films are very close in the paramagnetic regime, likely suggesting similar resistive behavior of the GB, despite their different structures. As the temperature is lowered, the resistivities of the HT and LT films diverge. A transition to a metallic state is observed at a temperature T_{MI} below T_C for the LT film. Such a transition also occurs in the HT film, but in a smoother way and even at lower temperature. Furthermore, a metal-to-metal transition is also observed at a temperature $T_2 = 130$ K in the HT film. For temperatures below 250 K and above 50 K, the resistivity of the HT film is far higher than the LT film's one. Similarities and differences in the resistive behaviors of these two films are more clearly evidenced in the temperature dependence of $\partial\rho/\partial T$ represented in Figure 13b. For $T \approx T_C$, we have $\partial^2\rho/\partial T^2$ for both HT and LT films. This inflection point of the resistivities reflects the onset of a magnetic order inside the columns, associated with an enhanced effectiveness of the double-exchange conduction mechanism. However, metallic behavior (i.e., $\partial\rho/\partial T > 0$) is only observed for $T = T_{MI}$ which is 20 and 35 K below T_C for the LT and HT films, respectively. The discrepancy between T_C and T_{MI} is probably due to the dominating increase of GB resistivity as the temperature is lowered from T_C to T_{MI}.[24] The domination of the GB resistivity over the intrinsic resistivity of the material comes to an end at a temperature 15° higher in the LT film, evidencing the different nature of the GB in the two films. Moreover, an accident in the $\partial\rho/\partial T$ curve, observed at $T = T_2$ only for the HT film, indicates a rapid increase of the conductivity as the temperature is decreased. Finally, at low temperature, the resistivities of the two films are again very close, the GB of the HT film reaching the same resistive state as the GB in the LT film. GB resistivity has been shown to strongly depend on temperature in the HT film. The observed transition at $T = T_2$ suggests the appearance of a magnetic order in the GB phase associated with a depressed Curie temperature, as compared to that of the column material. However, the resulting conduction mechanism in the GB still needs to be established. As mentioned above, double exchange is a possible mechanism, but so is spin tunneling. In the latter case, the loss of spin coherence near the interfaces between ferromagnetic electrodes and the insulating layer in tunnel junctions has been thought to be the cause for the absence of tunneling magnetoresistance above 75 K.[25] In our case, the onset of magnetic order in insulating GB could reinforce the spin coherence near the column's boundaries, giving rise to an enhanced tunneling rate between columns with parallel magnetization. Nevertheless, the metallic behavior of the HT films at very low temperature does not favor the tunneling mechanism, as an increase of the resistance below 50 K is usually associated with intergrain tunneling.[26,27] Magnetic scattering due to a spin-glass such as state of the GB can also be ruled out, as indicated by the transition toward a less resistive state at low temperature. Another indication of the absence of tunneling in the HT film is given by magnetoresistance measurements. Intergrain tunneling has indeed been made responsible for large changes of the resistance observed for fields of the order of the coercive field.[27] The resistance dependence on a magnetic field applied at $T = 30$ K in the substrate's plane is represented in Figure 14. The magnetotransport behavior is strikingly different for the LT and HT films and hence strongly depends on the microstructure. The LT film exhibits a quasi-linear and reversible variation of the resistance with the field reminiscent of the one observed for single crystals.[27] The magnetoresistance of the HT film measured from the demagnetized state is, on the contrary, highly irreversible, with a ratio $\rho(7T)/\rho(0T)$ twice that of the LT film. After the application of 7 T, the magnetoresistance exhibits a reversible butterfly wing shape. The 15% change in the resistivity between the demagnetized and remnant state is certainly associated with a different micromagnetic state. One could argue that upon cooling from T_C the magnetic domain configuration is established far above the magnetic transition temperature of the GB, i.e., while no direct magnetic exchange exists between columns. Due to their small size, and with neglect of any eventual magnetocrystalline anisotropy with respect to their shape anisotropy, the columns then probably correspond to single domains with the magnetization along their long axis. Magnetostatic consideration then leads to an antiparallel arrangement of the columns. Below T_2, the onset of magnetic interactions in GB would result in the presence of a large number of domain walls (DW) between antiparallel columns associated with a high scattering rate and a high resistive state. Upon the application of the field perpendicular to the columns, the magnetization rotates toward the field direction in the columns, but DW annihilation would occur only for a small misorientation between the moments of adjacent

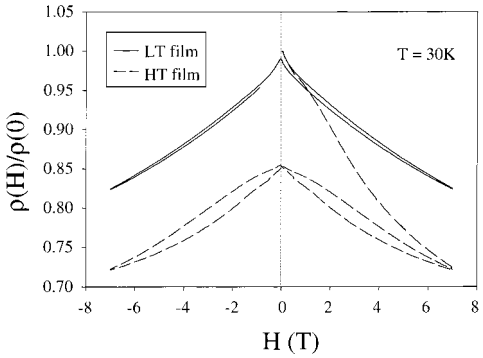

Figure 14. Magnetoresistance versus magnetic field. Data were taken at 30 K.

(23) Hejtmanek, J.; Jirak, Z.; Sedmidubsky, D.; Maignan, A.; Simon, Ch.; Caignert, V.; Martin, C.; Raveau, B. *Phys. Rev. B* **1996**, *54*, 11947.
(24) Mahesh, R.; Mahendiran, R.; Raychaudhuri, A. K.; Rao, C. N. R. *Appl. Phys. Lett.* **1996**, *68*, 2291.
(25) Sun, J. S.; Gallagher, J.; Ducombe, P. R.; Krusin-Elbaum, L.; Altman, R. A.; Gupta, A.; Gong, G. Q.; Xiao, G. *Appl. Phys. Lett.* **1996**, *69*, 3266.
(26) Ranno, L.; Llobet, A.; Hunt, M. B.; Pierre, J. *Appl. Surf. Sci.* **1999**, *138−139*, 228.
(27) Hwang, H. Y.; Cheong, S. W.; Ong, N. P.; Batlogg, B. *Phys. Rev. Lett.* **1996**, *77*, 2041.

columns, i.e., in a sufficiently high field. The application of 7 T is probably sufficient to align almost completely the magnetization in the columns, which are now directly interacting through the GB. This mechanism would explain the strong irreversibility of the virgin magnetoresistance. Furthermore, the hysteric behavior of the magnetoresistance observed in the HT film after the first field application, and absence of the LT film, could also be correlated to the pinning of DW by the GB where the magnetic exchange constant J is lower than that in the columns ($J \propto T_C$), leading to a minimized energy for the DW. Finally, no large low-field magnetoresistance could be evidenced, which is another indication of the absence of spin tunneling in the GB.

IV. Concluding Remarks

We have shown that high-quality thin films of the CMR manganite $Pr_{0.7}Sr_{0.3}MnO_3$ can be prepared using the PLD technique. Moreover, we have evidenced the great sensitivity of the orientation of the films and their microstructure to the substrate temperature. It is indeed remarkable that an increase of the deposition temperature by 20 °C, from 620 to 640 °C, changes dramatically the microstructure of the film and its orientation. Consequently, controlling carefully the temperature of the substrate, at 620 °C, well-crystallized [101]-oriented thin films with closely connected grains, i.e., scarcely visible grain boundaries, can be deposited. In contrast, for a substrate temperature of 640 °C, large platelet-like crystals, not well connected, with [101] and [010] domains are obtained.

Finally, it is worth pointing out that the PLD technique leads to much better results quality manganite thin films than sputtering techniques,[14] whose films were shown to exhibit only small size grains with poor interconnections.

Acknowledgment. We acknowledge Dr. M. Korzenski for helpful discussions. W.P. thanks Dr. R. L. Greene for his useful comments.

CM000206Z